Cement and Concrete Research 90 (2016) 174–183

Contents lists available at ScienceDirect

Cement and Concrete Research

journal homepage: www.elsevier.com/locate/cemconres

Compressive fatigue damage and failure mechanism of fiber reinforced cementitious material with high ductility

Qinghua Li [a], Botao Huang [a], Shilang Xu [a,*], Baomin Zhou [a], Rena C. Yu [b]

[a] Institute of Advanced Engineering Structures and Materials, Zhejiang University, Hangzhou, China
[b] ETSI de Caminos, Canales y Puertos, Universidad de Castilla-La Mancha (UCLM), Ciudad Real, Spain

ARTICLE INFO

Article history:
Received 16 January 2016
Received in revised form 26 May 2016
Accepted 20 September 2016
Available online 7 October 2016

Keywords:
C. Fatigue
E. Fiber reinforcement
E. High-performance concrete
B. SEM
C. Mechanical properties

ABSTRACT

The fiber reinforced cementitious material with high ductility has potential use in particular environments and structures that undergo repeated or fatigue loads. In this study, a series of monotonic and fatigue tests were performed to investigate the compressive fatigue behavior of this material. It is found that the fatigue life of this material is higher than that of plain concrete and steel fiber reinforced concrete under the same stress level. In addition, the failure deformation of fiber reinforced cementitious material with high ductility under fatigue load was larger than the monotonic envelope, while the envelope coincides with the monotonic loading curve for concrete or fiber reinforced concrete. The failure surface and damage process were investigated and a new failure mode of polyvinyl alcohol fiber with crushed end was discovered. The fatigue failure surface could be divided into three regions, including fatigue source region, transition region and crack extension region.

1. Introduction

Fiber reinforced concrete is made by adding fibers into concrete matrix to improve its ductility. With fiber reinforced concrete widely applied in modern complicated structures, which is subjected to repetitive cyclic loads (e.g. automobile traffic, wind action and sea waves), the fatigue behavior of this material is also getting more and more attention. Numerous experiments have been conducted to study the fatigue behavior of fiber reinforced concrete [1–8]. Fiber reinforced cementitious material with high ductility is a kind of cementitious material reinforced by random distributed short fibers, which is also referred to as engineered cementitious composites (ECC) [9], strain hardening cementitious composites (SHCC) [10], polyvinyl alcohol (PVA) fiber reinforced cementitious composites (PVA-FRCC) [11], or ultra-high toughness cementitious composites (UHTCC) [12], and its use has been explored throughout the world. This material was proposed by Li and Leung and was designed with micromechanical principles [13]. UHTCC possesses the following characteristics: it is reinforced with short fibers with the corresponding volume fraction lower than 2.5%; the hardened composite exhibits significant pseudo strain-hardening and multiple-cracking behaviors with tensile strain capability above 3%; and it can keep the crack width below 100 μm even when the tensile strain achieves its maximum value [12]. This material has potential use in complicated environments and structures that are subjected to repeated or fatigue loads, such as airport runway, highway pavements, bridge decks and offshore platform, due to its high ductility [12,14–16] and durability [17–20]. To apply ultra-high toughness cementitious composites in practice, the investigation of fatigue behavior of this material is needed.

Several studies have been carried out focusing on fatigue behavior of UHTCC in the past decade. Fatigue failure characteristics and fiber bridging characteristics of UHTCC under flexure were investigated and it was found that UHTCC exhibited significantly higher fatigue life and more ductility than concrete, polymer cement mortar and steel fiber reinforced concrete [21–25]. In addition, flexural fatigue behavior of concrete beam with UHTCC layer [26–28] and the tensile failure property of UHTCC under monotonic and cyclic tensile loads [29,30] has been studied. Based on the fatigue test results in [27], while the use of UHTCC layer can increase the strength of concrete beam, its improvement on fatigue performance is even more effective and concrete beam with UHTCC layer could sustain fatigue loading at a larger deflection without failure. Up to now, the existing study is mainly focused on the behavior of UHTCC under flexural fatigue and cyclic tensile loads, while there is limited study on the compressive fatigue properties of UHTCC. Considering that the fatigue behavior of UHTCC under compression is crucial for its application in certain conditions (e.g. airport runway and road pavements) and fatigue damage of structural components are affected by both the flexural and compressive cyclic loading, the available work is rather limited and a better understanding of the compressive fatigue behavior is required.

Thus, in order to investigate the fatigue behavior of UHTCC under compression, a series of monotonic and fatigue tests were performed.

* Corresponding author.
E-mail addresses: liqinghua@zju.edu.cn (Q. Li), botaohuang@zju.edu.cn (B. Huang), slxu@zju.edu.cn (S. Xu), zbmzjg@zju.edu.cn (B. Zhou), rena@uclm.es (R.C. Yu).

http://dx.doi.org/10.1016/j.cemconres.2016.09.019
0008-8846/

Table 1
Properties of PVA fiber.

Tensile strength (MPa)	Diameter (μm)	Fiber length (mm)	Young's modulus (GPa)	Elongation (%)
1600	40	12	40	6

This paper focuses on the evaluation of failure process of UHTCC, including fatigue life, deformation pattern and failure mode of fibers on the failure plane. Emphasis will be placed on analysis of the damage process of this material under monotonic and fatigue loads. Finally, relevant conclusions are drawn, which could be used as a reference for a wider application of UHTCC in structures.

2. Experimental program

2.1. Specimen preparation

In this experiment, UHTCC was produced using cementitious binders, fine silica sand, water, superplasticizer and PVA fiber [12]. The binders were composed of ordinary Portland cement and fly ash. The PVA fiber was KURALON K-II REC15 type with corresponding properties given in Table 1 and fibers added to the mix were 2% of the total composite volume. Two series of UHTCC cylinder specimens (Series I and II) with the same mix were prepared, the dimensions of which were 70 mm (diameter) × 140 mm (height). The specimens were demolded 72 h after they were cast and were cured for 28 days. Then, the specimens were laid in common environment for 3 months before monotonic and fatigue test.

2.2. Testing method

The compressive and fatigue test were performed in a 1000 kN INSTRON testing system. The displacement between two load platens was measured. For monotonic tests, displacement control was adopted with a constant rate of 0.20 mm/min. The average static compressive strength of Series I was 43.08 MPa (6 specimens), while that of Series II was 38.22 MPa (10 specimens). The average elastic modulus was 15 GPa measured by strain gauges during the static test. It needs to be pointed out that, although the elastic modulus of UHTCC is lower than that of concrete, this material could be applied to partially replace concrete at some crucial locations of structures to take the advantage of both materials. For fatigue tests, a constant amplitude fatigue load was used. The tests were carried out under load control with a sinusoidal waveform of 4 Hz. Six different stress levels were considered. Those maximum stress levels were 0.90, 0.85, 0.80, 0.75, 0.70 and 0.65, respectively, of the static compressive strength of UHTCC, shown in Table 2. Note that Series I was used in the fatigue tests under the stress level of 0.90, 0.80, 0.70 and 0.65, and Series II was used for the remaining stress levels. The ratio between the minimum fatigue loads to the maximum fatigue load ($R = P_{min}/P_{max}$) was kept at 0.1. The fatigue test commenced with a ramp to the maximum load at a rate of 8 kN/s followed by a sine waveform fatigue loading.

After specimen failure, the crushed pieces on the failure surface of specimens were selected for scanning electronic microscope (SEM) tests and Energy-dispersive X-ray spectroscopy (EDS) was utilized for the elemental analysis, as well as point analysis from the sample surface.

Table 2
Fatigue load and specimen numbers of the test.

Stress levels	Specimen series	Static compressive strength (MPa)	Maximum fatigue stress (MPa)	Specimen numbers
0.90	I	43.08	38.76	6
0.85	II	38.22	32.50	6
0.80	I	43.08	34.47	6
0.75	II	38.22	28.68	6
0.70	I	43.08	30.16	6
0.65	I	43.08	28.00	2

Table 3
Test result for fatigue life of UHTCC at various stress levels.

Specimen No.	Stress levels					
	0.90	0.85	0.80	0.75	0.70	0.65
1	620	1500	9520	42,524	484,135	2,000,000*
2	700	1869	28,394	149,691	679,756	2,000,000*
3	1100	1928	35,908	497,273	1,054,123	/
4	1572	4052	55,629	718,343	1,906,379	/
5	1586	4115	108,081	792,262	2,000,000*	/
6	1900	13,019	131,442	1,295,229	/	/

Note: * represents the fatigue failure did not happen when load cycles reached two million.

3. Results and discussion

3.1. Fatigue life and distribution

The fatigue lives for each fatigue stress level are summarized in Table 3, which were obtained from the above experiment study. Note that specimens that did not fail at two million cycles are considered as run-outs. Since the fatigue life distribution of plain and fiber reinforced concrete was found previously to follow the Weibull distribution in [7,8,31–33] and the flexural fatigue life of UHTCC follows this distribution as well [25], in this paper, the verification of Weibull distribution will be attempted for compressive fatigue of UHTCC.

For fatigue life, the Weibull cumulative distribution function $P_f(N)$ could be written as follows with the location parameter or minimum value considered as zero [31–33].

$$P_f(N) = 1 - \exp\left[-\left(\frac{N}{N_a}\right)^{\alpha}\right] \tag{1}$$

where α is the shape parameter; N_a is the scale parameter; N is the fatigue life.

Taking twice natural logarithm for both sides of Eq. (1) gives

$$\ln \ \ln \frac{1}{1-P_f(N)} = \alpha \ln \ N - \alpha \ln \ N_a \tag{2}$$

Setting $Y = \ln \ln (1/(1 - P_f(N)))$, $X = \ln N$, $\beta = \alpha \ln u$, we can get

$$Y = \alpha X - \beta \tag{3}$$

The graphical method could be employed to estimate the distribution parameters and it could be found from Eq. (3) that the fatigue lives follow Weibull distribution when the relationship between Y and X is linear (the correlation coefficient r is close to one). Also, when a failure probability p is given, the corresponding fatigue life N at certain stress level S could be calculated.

According to the probability theory of Weibull distribution, the failure probability p corresponding to the tested failure life N can be

Table 4
The results of Weibull distribution parameters and regression analysis.

Stress levels	α	β	r	N_a
0.90	1.9054	13.8900	0.9661	1465
0.85	1.0249	8.7558	0.8941	5131
0.80	0.9429	10.5593	0.9891	73,039
0.75	0.6979	9.4061	0.9722	713,344
0.70	1.3936	19.5555	0.9769	1,242,160

Table 5
Fatigue equations of UHTCC, plain concrete and SFRC.

Materials	Fatigue equation
UHTCC	$S = -0.0670 \log N + 1.0360$ ($p = 0.05$, $r = 0.9625$)
	$S = -0.0618 \log N + 1.0837$ ($p = 0.50$, $r = 0.9864$)
	$S = -0.0555 \log N + 1.0877$ ($p = 0.95$, $r = 0.9653$)
Plain concrete of Eq. (5) [34]	$S = -0.0617 \log N + 1.0000$
Plain concrete of Eq. (6) [35]	$S = -0.0765 \log N + 1.0578$
SFRC (0.5 vol%) [6]	$S = -0.0632 \log N + 0.9987$
SFRC (1.0 vol%) [6]	$S = -0.0497 \log N + 0.9697$
SFRC (0.57 vol%) [5]	$\log S = -0.0566 \log N + 0.0918$

Note: vol% means the percentage of steel fibers by volume of concrete.

expressed by

$$p = \frac{i}{k+1} \quad (i = 1,\ 2, \ldots,\ k) \tag{4}$$

where, k is the total number of the fatigue test data at certain stress level; i is the sequence number of failure specimens at certain stress level. Then the linear regression is carried out for the fatigue test data according to Eq. (3). Table 4 shows the results of the Weibull distribution parameters and regression analysis for UHTCC compressive fatigue life. Note that for a stress level of 0.70, there was one runout test, only four tests were used to obtain the probabilistic fitting.

It is found in Table 4 that all correlation coefficients are between 0.8941 and 0.9891, which indicates that the relationship between X and Y is linear for all stress levels. This validates that the compressive fatigue lives of UHTCC in this study follow the Weibull distribution. Moreover, the single-logarithmic fatigue equations of UHTCC of various failure probabilities could be obtained, which is shown in Table 5. The test data and fatigue equations are plotted in Fig. 1 and the arrow in this figure indicates that the fatigue failure did not happen when load cycles reached two million. It could be found that almost all of the test data are in the region between 5% and 95% failure probability in Fig. 1. In addition, similar to concrete, the variability becomes larger for lower fatigue stress level [32], which is indicated by the fatigue equations, and this effect should be considered during the application of UHTCC.

For the sake of comparison, several fatigue equations of plain concrete and steel fiber reinforced concrete (SFRC) are shown in Table 5. For plain concrete, the classical S—N fatigue equation [34] is as follows:

$$\frac{\sigma_{max}}{f_c} = 1 - (1-R)\beta \log N \tag{5}$$

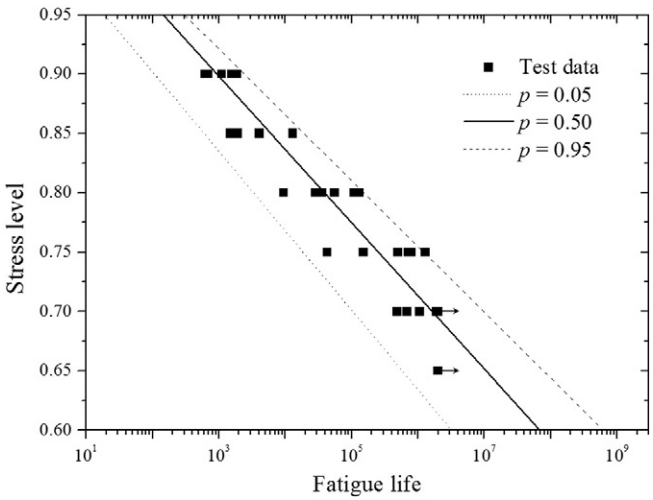

Fig. 1. Experimental fatigue life and fatigue curves of UHTCC.

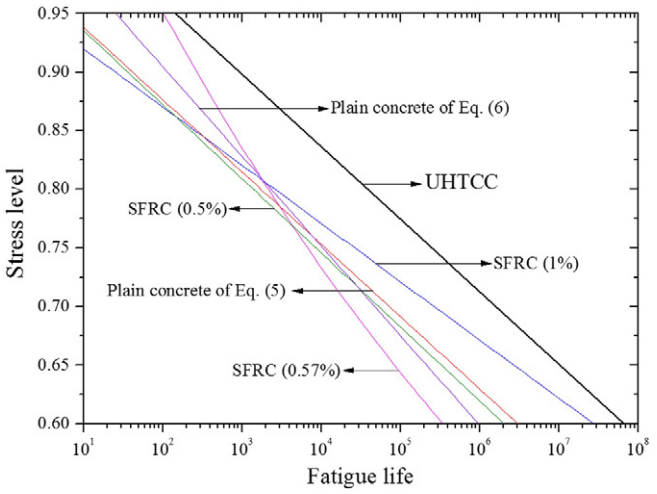

Fig. 2. S - N curves of UHTCC, plain concrete and steel fiber reinforced concrete under compression fatigue load.

where σ_{max} is the maximum stress in fatigue test; f_c is the static compressive strength; β is a material parameter, it equals 0.0685. Another improved model was developed by Zhang et al. [35], including loading frequency and reversal stresses as expressed in the Eq. (6):

$$\frac{\sigma_{max}}{f_c} = \left(ab^{-\log f} + c\right)[1-(1-R)\beta \log N] \tag{6}$$

where a, b, c and β are material parameters, which equals 0.249, 0.920, 0.796 and 0.0804, respectively; and f is the loading frequency. The above equations of plain concrete in Table 5 was obtained of $R = 0.1$ and $f = 4$ Hz. For steel fiber reinforced concrete (SFRC), the equations in [5,6] are used. Note that, the single-logarithmic fatigue equations in [6], which is an overview article, came from the test data published in [2–4,36]. Meanwhile, the double-logarithmic fatigue equation of SFRC (0.57 vol%) came from [5], which showed the longest fatigue life at the same stress level in that study. In Fig. 2, the S - N curves of UHTCC, plain concrete and steel fiber reinforced concrete are plotted. It should be noted that the curve of UHTCC is from single-logarithmic fatigue equation when failure probability is 0.50 and the curve of SFRC (0.57 vol%), which is not linear in Fig. 2, comes from its double-logarithmic fatigue equation.

Although there are numerous combinations which can influence the fatigue behavior of plain concrete and steel fiber reinforced concrete, due to the numerous sources of fatigue data analyzed, the qualitative trends observed should be generally applicable [6]. Hence, it could be

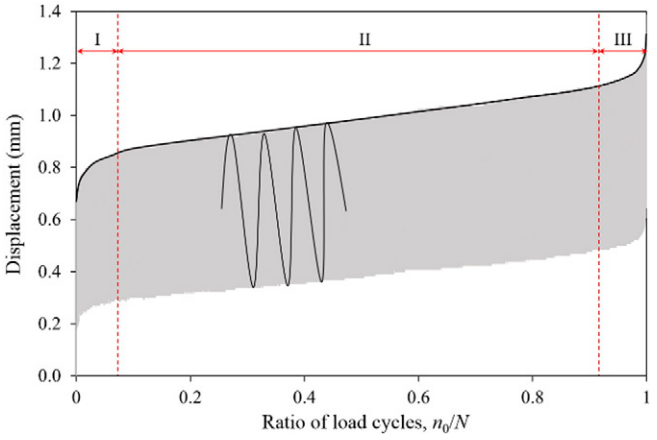

Fig. 3. Evolution curves of deformation of fatigue specimen with ratio of load cycles.

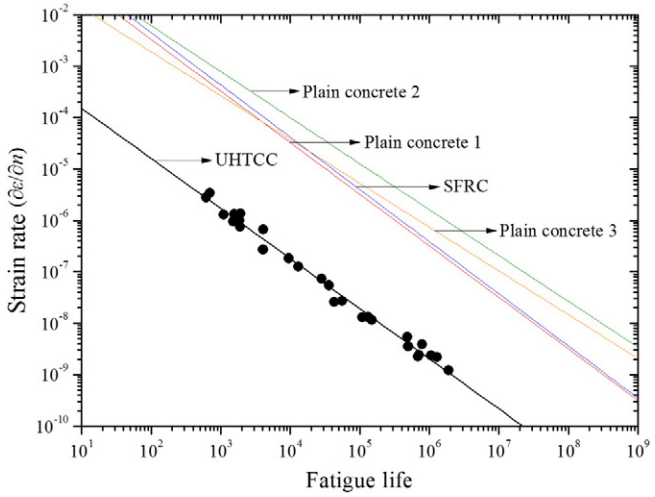

Fig. 4. Secondary strain rate versus fatigue life.

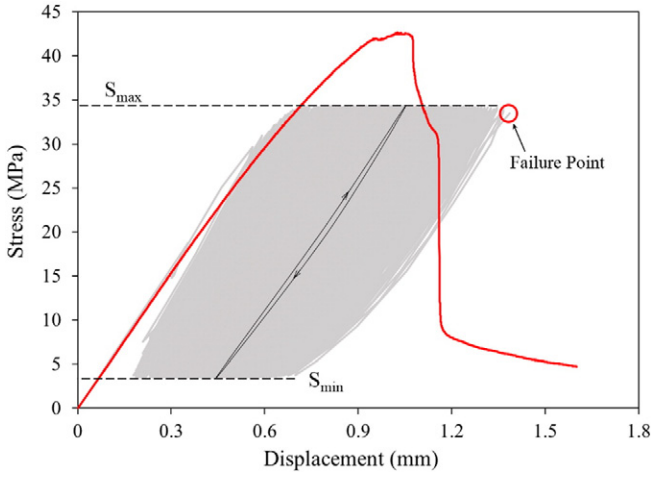

Fig. 5. Comparison of maximum displacement at fatigue failure of UHTCC (S = 0.80) with monotonic envelope.

seen that the fatigue life of UHTCC is higher than that of plain concrete and steel fiber reinforced concrete under the same stress level.

This phenomenon might be related to the relatively higher fiber percentage of fibers by volume (2 vol%) of UHTCC, due to the fact that the fibers can bridge cracks thus contribute to substantially enhance the post-peak behavior in compression [16]. That is to say, a possible explanation is that UHTCC owns higher toughness and ductility compared with plain concrete and steel fiber reinforced concrete. Also, further experimental work and study are required to understand the mechanism of this phenomenon.

3.2. Monotonic and fatigue failure deformations

Fig. 3 shows a typical evolution curve of compressive displacement of fatigue specimen (0.8–1) with respect to the normalized load cycles and three stages of deformation are observed : (I) rapid developing stage; (II) stable developing stage; and (III) failure stage. During the rapid developing stage and the failure stage, each contributed to 5–10% of fatigue life while the deformation increased significantly. The second stage covered 80–90% of the total fatigue life, where the deformation of specimen stably augmented. Similar phenomenon can be found for all of the rest specimens for stress levels from 0.70 to 0.90.

At the stable developing stage, an approximately linear branch can be observed and a strong correlation exists between the slope of the secondary creep branch, the secondary strain rate, and the number of cycles to failure [5,7,8,36]. Considering that the value of the secondary strain rate is related to the loading frequency of the fatigue test, for the sake of comparison, we used the rate of strain increase per cycle of the secondary creep branch instead of the rate of strain increase per second. The relationship between these two values is as follow:

$$\frac{\partial \varepsilon}{\partial t} = \frac{\partial \varepsilon}{\partial (t \times f)} \times f = \frac{\partial \varepsilon}{\partial n} \times f \tag{7}$$

where f is the loading frequency of each fatigue test.

Thus we can make comparison between various fatigue test results under different loading frequencies. As shown in Fig. 4, an excellent correlation can be observed for UHTCC and the coefficients of correlation is higher than 0.99. Also, another four curves of plain concrete and steel fiber reinforced concrete (SFRC) are presented. The curves of Plain concrete 1 and SFRC come from the results of specimen Series I in Reference [5] and the curves of Plain concrete 2 and 3 come from the results of Concrete A and B in [36], respectively. At the same secondary strain rate, the fatigue life of UHTCC is much smaller than that of plain concrete and SFRC. It indicates that, comparing with plain concrete and SFRC, micro cracks in UHTCC extend much slower in the secondary creep branch and this could also be an explanation for the reason why UHTCC owns higher fatigue life under the same stress level.

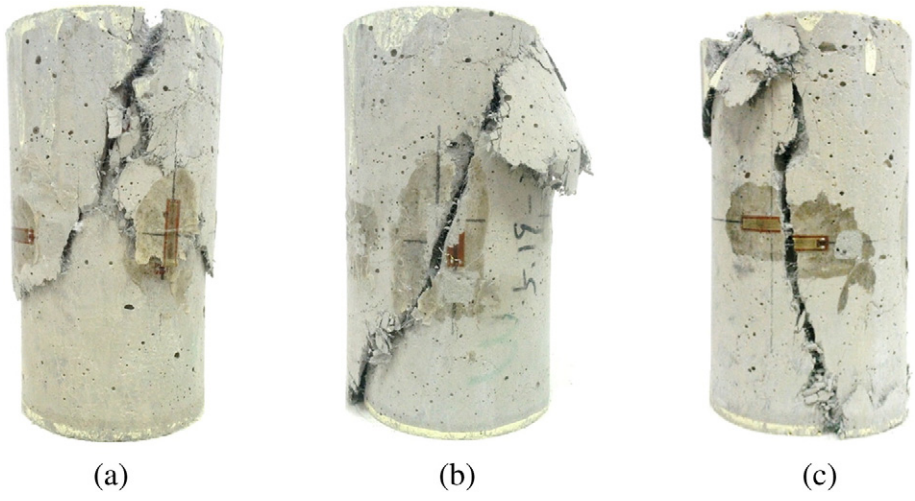

Fig. 6. Typical fatigue failure modes of cylindrical specimens under compression.

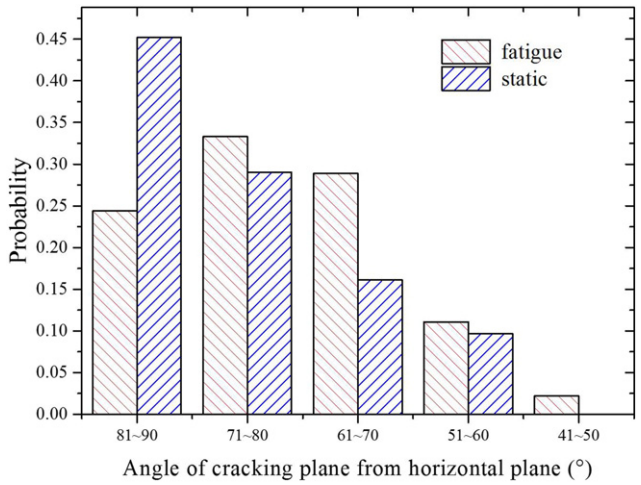

Fig. 7. Probability of angle of cracking plane from horizontal plan.

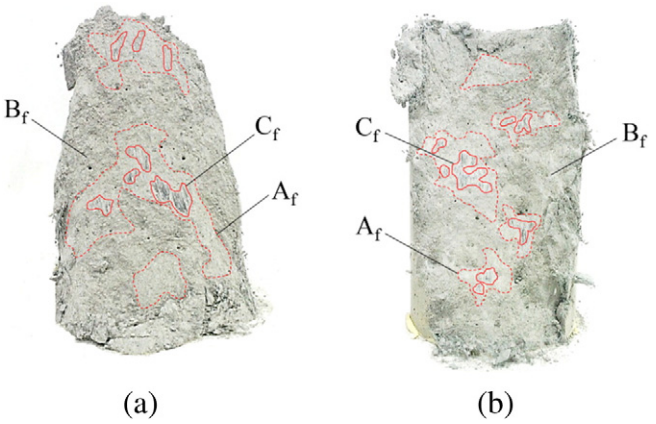

Fig. 9. Fatigue failure surface of UHTCC specimens.

The deformation corresponding to the maximum force of the last cycle supported by the specimen is regarded as the maximum deformation at fatigue failure. Generally, the fatigue behavior of plain concrete and steel fiber reinforced concrete, which is accepted in the literature, is the existence of an envelope for deformations [1,5,37]. The envelope coincides with that of the monotonic loading curve or, at least, is very close to it.

When it comes to UHTCC, however, there exists unexpected phenomenon. Compared with that of monotonic loading curve, the maximum deformation at fatigue failure appears to be much larger, as shown in Fig. 5, wherein the fatigue stress - displacement diagram of a specimen for stress level of 0.80 is plotted over a monotonic stress - displacement diagram for UHTCC of Series I. Although not presented in the figure, similar results were attained for all specimens subjected to stress levels from 0.70 to 0.90. Hence, for UHTCC, the monotonic stress-deformation diagram cannot be used as an envelope for fatigue deformations. In addition, this indicates that UHTCC owns higher deform ability and shows more ductility at fatigue failure compared with plain concrete and steel fiber reinforced concrete.

A possible explanation for the higher fatigue deformation of UHTCC compared with monotonic one is as follows. In the initial design of UHTCC, the interface of PVA fibers was treated. PVA fibers would not rupture during the fiber chemical debonding process owing to the strong slip-hardening effect during fiber pull-out [13,38], which also means that the treated PVA fibers are more amenable to bridge cracks. More micro cracks form and grow in the mix of UHTCC when subjected to fatigue load and a part of PVA fibers would be pulled-out during this process. Due to the slip-hardening effect, the fibers except the rupture ones would still be working and even bridge cracks more efficiently. That is to say, on one hand, more micro cracks forming, growing and being bridged lead to larger fatigue deformation. On the other hand, this also means the treated PVA fibers can prolong the fatigue life of UHTCC. However, this hypothesis needs to be studied further since numerous factors contribute to fatigue deformation and life.

3.3. Fatigue damage mechanism

3.3.1. Fatigue failure mode

Typical fatigue failure modes of UHTCC specimens under compression are shown in Fig. 6. It can be seen that major inclined shear cracks formed along the specimens with the cracking plane inclined approximately 60–90° with respect to the horizontal plane and the specimen did not burst into pieces after failure, which is different from that of concrete and similar to steel fiber reinforced concrete [39]. The static and fatigue failure modes of UHTCC are similar and it could be attributed to the bridging interaction between PVA fibers and the cementitious matrix, which kept the specimens in integrity after failure.

Fig. 7 shows the distributions of the angles of cracking plane from horizontal plane. These angles were divided into five regions (81–90°, 71–80°, 61–70°, 51–60°, 41–50°). It can be seen that, for specimens under static load, almost half of the major cracks formed along these specimens with the cracking plane 81–90° from the horizontal plane. However, the angle of cracking plane mainly falls within 61–80° for fatigue load. Under the external loads, micro cracks in specimen

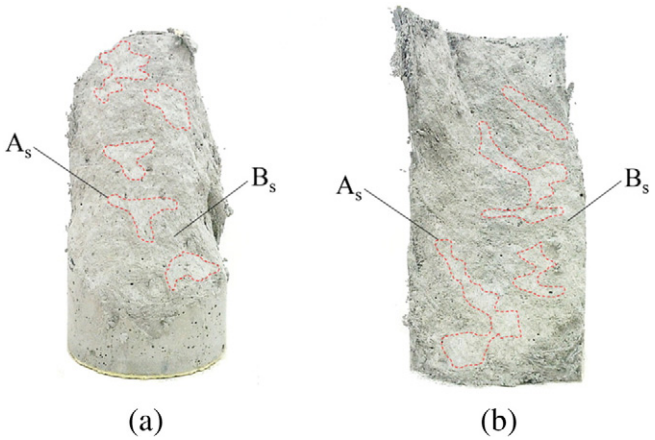

Fig. 8. Static failure surface of UHTCC specimens.

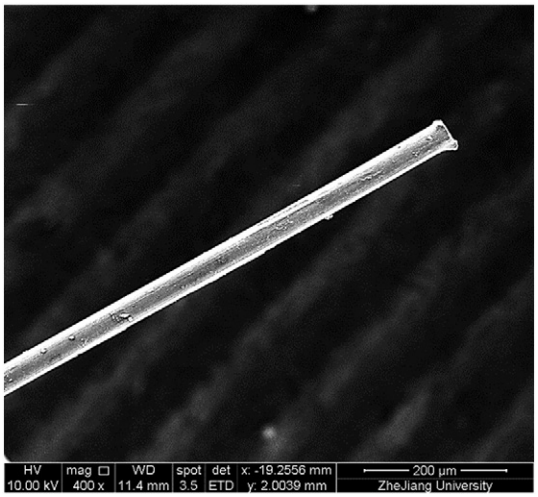

Fig. 10. SEM image of PVA fiber.

Fig. 11. SEM image of "flat" area on static failure surface (Region A_s).

continuously propagate to form main cracks or cracking planes. Note that, under fatigue load, more micro cracks may form and grow in the mix of UHTCC compared with those under static load. This indicates the main crack angles may have more choices under fatigue load and the angle distribution would be different from that under static loading.

3.3.2. Static and fatigue failure surface

To investigate the damage process of UHTCC, the failure surfaces of specimens under static and fatigue load are shown in Fig. 8 and Fig. 9, respectively.

For the static failure specimen, the failure surface can be approximately divided into two regions by macroscopic observations (Fig. 8). Region A_s ("s" stands for static), which is surrounded by dashed line, is a "flat" area wherein PVA fibers are practically not visible by the naked eyes, while Region B_s (the rest area of failure surface) is a "rough" area with numerous PVA fibers observed by the naked eyes.

By contrast, three distinct regions can be identified by macroscopic observation for the fatigue failure surface. As shown in Fig. 9, similar to the static failure surface, there exists "flat" areas named Region A_f ("f" stands for fatigue) surrounded by dashed line. PVA fibers are hardly observable by the naked eyes in these areas. Also, a "rough" area with numerous PVA fibers observed by the naked eyes named Region B_f. The emphasis would be placed on the area called Region C_f on the fatigue failure surface, which is surrounded by solid line inside of Region A_f. Different from Region A_f and A_s, this area is "darker" compared to the surrounding areas by macroscopic observation and there exists trace of "friction".

It needs to be pointed out that this way of dividing the failure surface is rather qualitative, which is to be used to analyze and get deeper understanding of the damage process in the following analysis. Note that there also might be some areas with the above features not being marked on the failure surfaces.

3.3.3. SEM analysis

Scanning electron microscopy (SEM) was performed to study the failure modes of PVA fibers on various regions of the static and fatigue failure surface. Fig. 10 illustrates the initial shape of a single PVA fiber, which could be used as a reference in the following analysis, and the SEM images of the regions on failure surface are shown in Fig. 11, Fig. 12, Fig. 13, Fig. 15 and Fig. 16.

The static failure surface has been divided into two regions with SEM images shown in Fig. 11 (Region A_s) and Fig. 12 (Region B_s). The fibers in Fig. 11 have been marked and it can be seen that most of the fibers were ruptured (e.g. Fiber 1 in Fig. 11 (b), Fiber 3 & 4 in Fig. 11 (c)) and a small part of them were pulled-out (e.g. Fiber 2 in Fig. 11 (b)). The shape of pull-out and ruptured fibers are very close to that of the fibers damaged by pullout test in [38]. It indicates that the reason why Region A_s were "flat" in macroscopic observation might be related to the fact that most of the fibers were ruptured with short end leaving outside of mix. By contrast, Region B_s (Fig. 12) exists numerous damaged fibers with pull-out end, while the fibers with ruptured end existed with a low proportion. The traces of fibers could also be observed clearly in Fig. 12 (a), which is evident that the fibers were mainly damaged by pull out. Note that the pull-out fiber would leave a longer end on the failure surface compared with a ruptured one. Thus, the "roughness" of Region B_s can be attributed to the fact that the ratio of pull-out fibers is high.

For the fatigue failure surface, which has been divided into three regions, the SEM images are shown in Fig. 13 (Region C_f), Fig. 15 (Region A_f) and Fig. 16 (Region B_f). The emphasis would be placed on Region C_f,

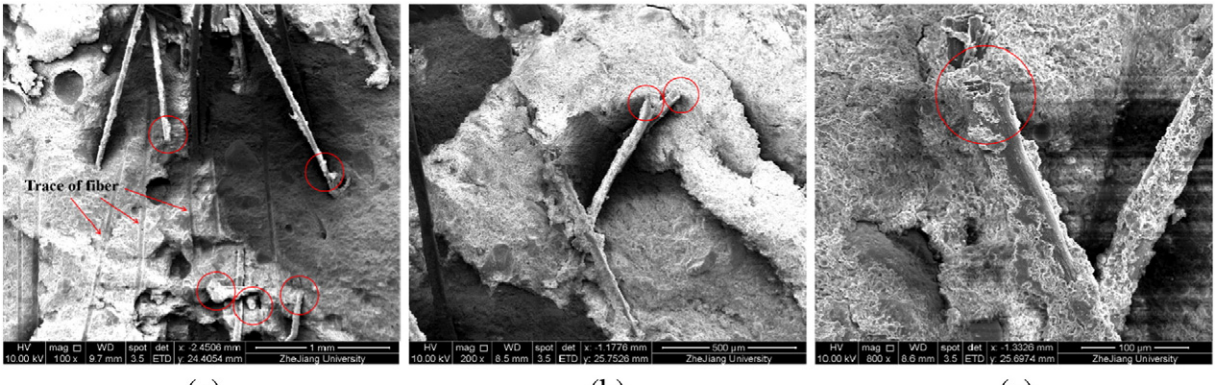

Fig. 12. SEM image of "rough" area on static failure surface (Region B_s).

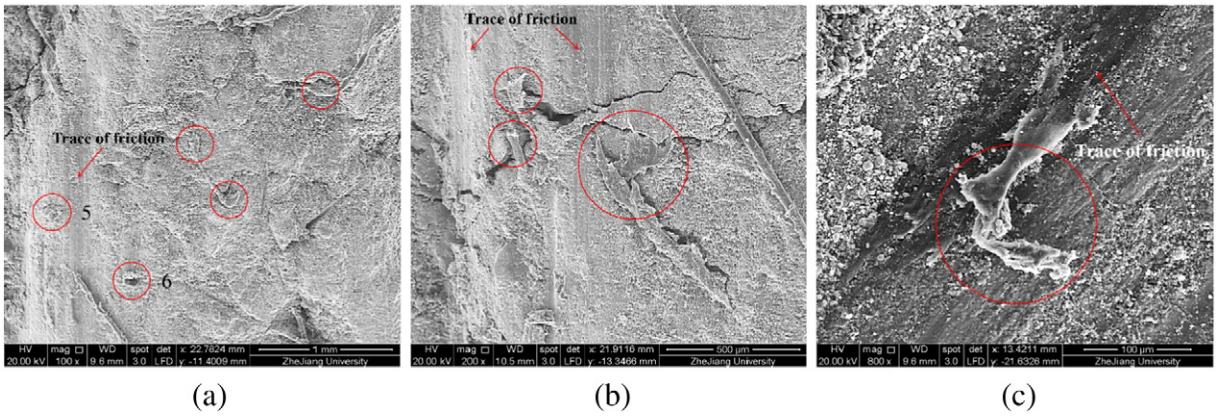

Fig. 13. SEM image of "flat & darker" area on fatigue failure surface (Region C_f).

which is "darker" in macroscopic observation and shows different characteristics compared to the static failure surface. A new damage mode of fibers can be found in Region C_f and it seems that these fibers suffered from crushing. In Fig. 13, to confirm Mark 5 and 6 are PVA fibers, energy-dispersive X-ray spectroscopy (EDS) is utilized for the preliminary analysis. The corresponding results are shown in Fig. 14, which indicates they are PVA fibers due to the high concentration of Carbon. It should be noted that there exists clear trace of "friction" in Region C_f, which has been mentioned above, and this trace of "friction" could also be found in SEM images. It means that the new damage mode of fibers might be related to the trace of "friction". A possible explanation for the formation of the new damage mode of fibers might be that the damaged fibers were ruptured in the early stage of the fatigue failure process and the ruptured end suffered from repeated friction or crushing during the rest fatigue life. In the following part, this fiber end damage type can be named as crushed end. There are two fiber damage modes in Region A_f (Fig. 15). Part of the fibers were crushed (e.g. Fiber 7), while the others were ruptured (e.g. Fiber 8). Similar to Region A_s (static failure), Region C_f and A_f was "flat" in macroscopic observation owing to most fibers were ruptured or crushed (lying very close to the failure surface). The reason why Region C_f is "darker" is still unknown and it may be a result of friction or crushing. Further investigation is needed to explain this phenomenon. Finally, for Region B_f (Fig. 16), the fibers with pull-out end (e.g. Fiber 9 & 10 in Fig. 16 (b)) existed with high proportion, while the fibers with ruptured end (e.g. Fiber 11 in Fig. 16 (c)) existed with low proportion. Thus, it is found that the characteristics of Region B_f and B_s are quite similar. Further discussion of the relationship between static and fatigue failure surface and damage process will be given in the following section.

3.3.4. Discussion of the static and fatigue damage process

Based on the above region division of static and fatigue failure surface and the results of SEM analysis, the damage processes in UHTCC under cyclic loading are illuminated.

The possible static failure process of UHTCC is as follows. As the monotonic external loading increased, considering that the PVA fibers are random distributed in mix, the regions with less fibers show higher probability to form micro cracks due to the lack of enough bridge force. In the early period of static failure, micro cracks of these regions grow slowly and the deformation of the specimen is small. It should be noted that the rupture damage of PVA fibers can happen in smaller deformation condition compared with pull-out damage. Hence, the fibers, which bridged the appeared micro cracks, will mainly be ruptured in the early stage of failure. With the loading increasing, cracks continually extend and the deformation of specimen becomes larger. Beyond the peak load, the ratio of pull-out fibers increases and bridging effect of fibers becomes more active during this period.

From the above analysis of static failure process and failure surfaces, it could be concluded that Region A_s can be regarded as the region wherein micro cracks began to initiate with the fibers ruptured. Moreover, Region B_s with numerous fibers pulled out is formed by the extension of cracks beyond the peak load. Thus, the static damage of UHTCC specimen occurs, when the crack propagated from Region A_s to B_s, and it also explains the formation of the fiber failure modes in these

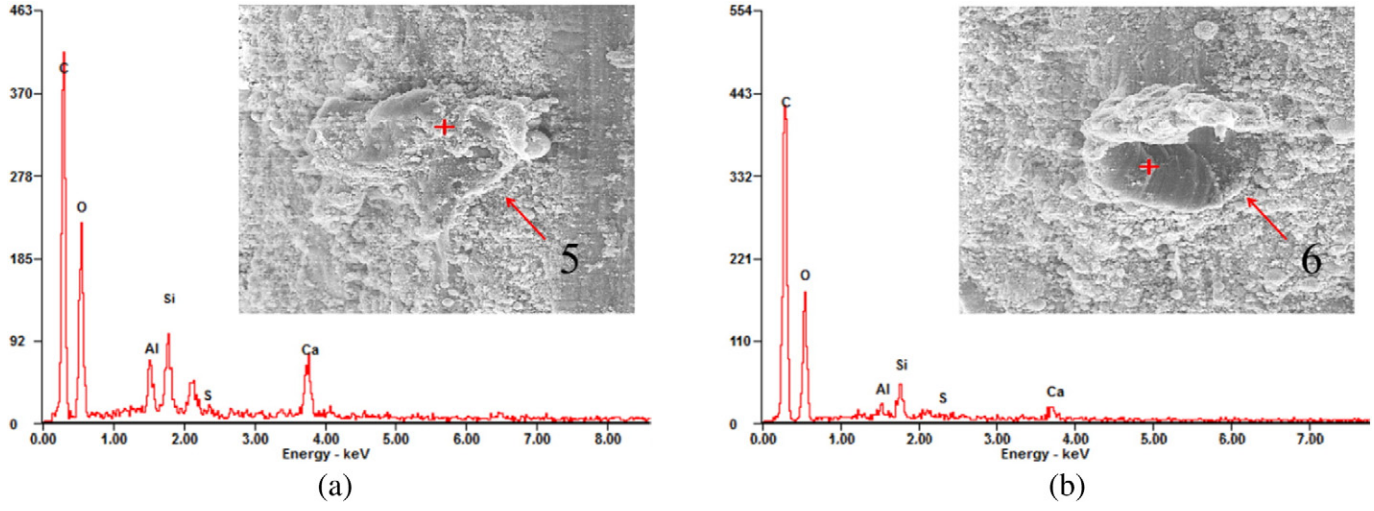

Fig. 14. EDS analysis of the marked points.

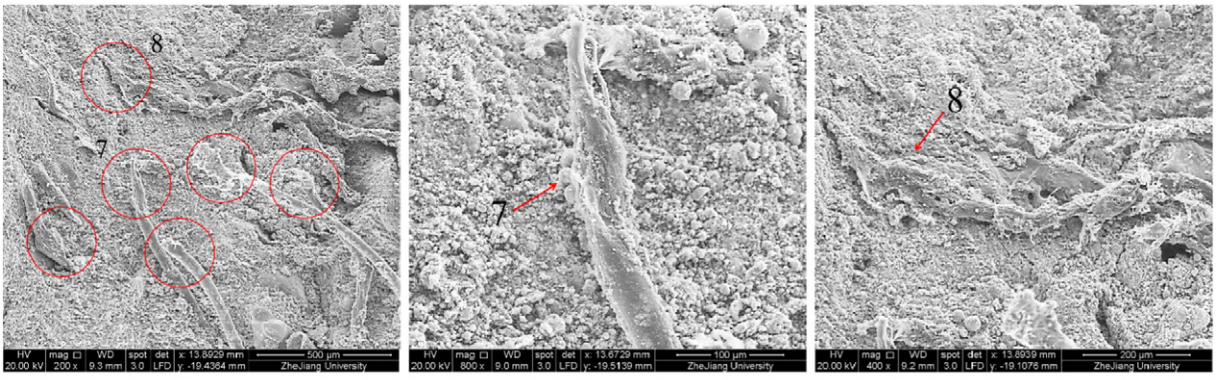

Fig. 15. SEM image of "flat" area on fatigue failure surface (Region A_f).

regions. Note that the above failure process is based on qualitative analysis and further studies are still required.

In addition, knowledge on the static failure process can give us insight on the understanding of the fatigue failure process. In the early stage of fatigue damage, the micro cracks appear and propagate slowly and the deformation of the specimen is small, which are similar to that of a static damage process. Moreover, the fibers would mainly be ruptured in this stage. Then, the ruptured end of fibers in the formed cracks would experience repeated crushing and friction from the mix due to the external fatigue load. This process distinguishes the fiber failure mode of fatigue damage from that of static damage and it also explains the reason why the fibers seems to be crushed and the trace of friction could be found in Region C_f. Looking back to the above process, the micro cracks could be regarded as the fatigue source. In other words, Region C_f could also be regarded as the fatigue source region, which can be discerned by macroscopic observation. For the static and fatigue damage process, Region A_s and C_f are the region wherein micro cracks begin to initiate, respectively.

Following that, the cracks continuously propagate until fatigue failure occurs. Similar to the static damage, the cracks propagate from Region C_f to B_f in this process. It can be found that Region B_f is really close to Region B_s due to both of them formed in the later period of the failure process. During this period, the increased deformation of the specimen lead to the appearance of pull-out damaged fibers. It should be noted that the difference between the static and fatigue failure is that there exists Region A_f on the fatigue damage surface. Remember that most of the fibers in Region A_f own crushed or ruptured ends, while the fibers in Region C_f mainly own crushed ends only and the fibers in Region B_f own pull-out or ruptured ends. Thus, Region A_f can be regarded as a transition area between Region C_f and Region B_f.

During fatigue damage process (shown in Fig. 17), micro cracks appear and propagate at the rapid developing stage (I). Then, Region C_f is formed at the stable developing stage (II), which is the fatigue source region with crush damaged fibers. After that, Region A_f (transition region) is formed at the failure stage (III). Finally, Region B_f formed around the last cycle with fibers pulled out and ruptured and can be denominated as crack extension region. In summary, micro cracks initiate in the fatigue source region, propagate in the transition region and form the main crack in the extension region.

Considering that the above discussion of the damage process is based on the qualitative analysis of the failure surface and SEM analysis, further evidence and investigation, as well as quantitative analysis, are indispensable. In addition, a more accurate method to distinguish the crack-initiating regions (Region A_s and C_f) is needed due to that the macroscopic observation in this paper is not as accurate as we would like. Also, the relationship between the fatigue deformation and the crack propagation need to be paid more attention to in future studies.

4. Conclusions

A series of monotonic and fatigue tests were performed in this study to investigate the fatigue behavior of ultra-high toughness cementitious composites under compression. The fatigue life of UHTCC specimens is shown to follow a Weibull distribution and the *S* - *N* relationship was given, which indicates that the fatigue life of this material is higher than that of plain concrete and steel fiber reinforced concrete under the same stress level. In addition, the maximum deformation of UHTCC at failure under fatigue load was larger than that of the monotonic envelope, while the envelope coincides with the monotonic loading curve for concrete or fiber reinforced concrete, and the fatigue life of

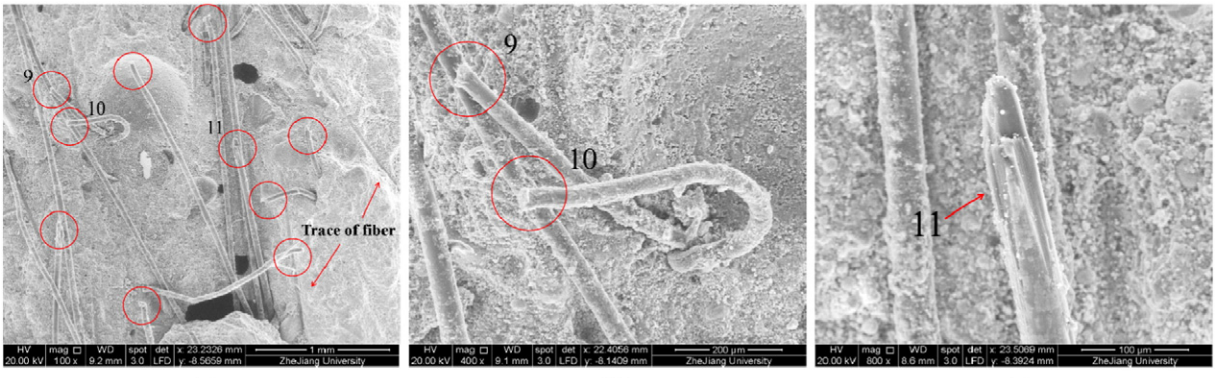

Fig. 16. SEM image of "rough" area on fatigue failure surface (Region B_f).

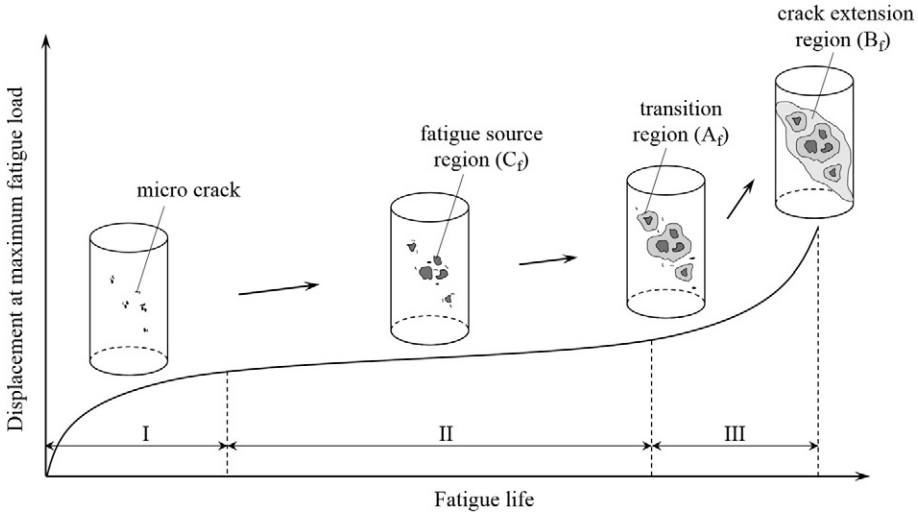

Fig. 17. Fatigue failure damage process of UHTCC specimen.

UHTCC is much smaller than that of plain concrete and fiber reinforced concrete at the same secondary strain rate.

The failure surface and damage process of UHTCC were investigated. A new failure mode of PVA fiber with crushed end was discovered with the help of SEM analysis and EDS analysis. This failure mode forms by the ruptured ends of fibers experiencing repeated crushing. The fatigue failure surface could be divided into three regions, including fatigue source region, transition region and crack extension region. During the fatigue failure process, micro cracks initiate in the fatigue source region, propagate in the transition region and form main cracks in the crack extension region.

Acknowledgement

The authors would like to acknowledge the financial supports provided by National Natural Science Foundation of China with grant No. 51378462 and 51008270. The authors appreciate the efforts of the anonymous reviewers to improve the quality of this study.

References

[1] D.E. Otter, A.E. Naaman, Properties of steel fiber reinforced concrete under cyclic loading, ACI Mater. J. 85 (4) (1988) 254–261.
[2] M. Grzybowski, C. Meyer, Damage accumulation in concrete with and without fiber reinforcement, ACI Mater. J. 90 (1993) 594–604.
[3] T. Paskova, C. Meyer, Low-cycle fatigue of plain and fiber reinforced concrete, ACI Mater. J. 94 (1997) 273–285.
[4] P.B. Cachim, Experimental and numerical analysis of the behaviour of structural concrete under fatigue loading with applications to concrete pavements, PhD thesis, Faculty of Engineering of the University of Porto 1999, p. 246.
[5] P.B. Cachim, J.A. Figueiras, P.A.A. Pereira, Fatigue behavior of fiber-reinforced concrete in compression, Cem. Concr. Compos. 24 (2) (2002) 211–217.
[6] M.K. Lee, B.I.G. Barr, An overview of the fatigue behaviour of plain and fibre reinforced concrete, Cem. Concr. Compos. 26 (4) (2004) 299–305.
[7] L. Saucedo, R.C. Yu, A. Medeiros, X. Zhang, G. Ruiz, A probabilistic fatigue model based on the initial distribution to consider frequency effect in plain and fiber reinforced concrete, Int. J. Fatigue 48 (2013) 308–318.
[8] A. Medeiros, X. Zhang, G. Ruiz, R.C. Yu, M.D.S.L. Velasco, Effect of the loading frequency on the compressive fatigue behavior of plain and fiber reinforced concrete, Int. J. Fatigue 70 (2015) 342–350.
[9] V.C. Li, From micromechanics to structural engineering-the design of cementitious composites for civil engineering applications, J. Struct. Mech. Earthq. Eng. 10 (2) (1993) 37–48.
[10] V.C. Li, T. Hashida, Engineering ductile fracture in brittle-matrix composites, J. Mater. Sci. Lett. 12 (12) (1993) 898–901.
[11] P.K. Nelson, V.C. Li, T. Kamada, Fracture toughness of microfiber reinforced cement composites, J. Mater. Civ. Eng. ASCE 14 (5) (2002) 384–391.
[12] H. Li, S. Xu, C.K.Y. Leung, Tensile and flexural properties of ultra high toughness cementitious composite, J. Wuhan Univ. Technol. 24 (4) (2009) 677–683 Mater. Sci. Ed.
[13] V.C. Li, C.K.Y. Leung, Steady state and multiple cracking of short random fiber composites, J. Eng. Mech. ASCE 188 (11) (1992) 2246–2264.
[14] V.C. Li, S. Wang, C. Wu., Tensile strain-hardening behavior of polyvinyl alcohol engineered cementitious composite (PVA-ECC), ACI Mater. J. 98 (6) (2001) 483–492.
[15] J. Zhou, J. Pan, C.Y.K. Leung, Mechanical Behavior of Fiber-Reinforced Engineered Cementitious Composites in Uniaxial Compression, J. Mater. Civ. Eng. ASCE 27 (1) (2015), 04014111.
[16] S. Xu, X. Cai, Experimental study and theoretical models on compressive properties of ultrahigh toughness cementitious composites, J. Mater. Civil Eng. ASCE 22 (10) (2010) 1067–1077.
[17] M.D. Lepech, V.C. Li, Long term durability performance of engineered cementitious composites, Int. J. Restor. Build. Monum. 12 (2) (2006) 119–132.
[18] M. Sahmaran, V.C. Li, Durability of mechanically loaded engineered cementitious composites under highly alkaline environment, Cem. Concr. Compos. 30 (2) (2008) 72–81.
[19] M. Sahmaran, M. Lachemi, V.C. Li, Assessing the durability of engineered cementitious composites under freezing and thawing cycles, J. ASTM Int. 6 (7) (2009) 1–13.
[20] S. Xu, X. Cai, Mechanics behavior of ultra high toughness cementitious composites after freezing and thawing, J. Wuhan Univ. Technol. 25 (3) (2010) 509–514 Mater. Sci. Ed.
[21] P. Suthiwarapirak, T. Matsumoto, T. Kanda, Flexural fatigue failure characteristics of an engineered cementitious composites and polymer cement mortars, J. Mater. Concrete Struct. Pavements 57 (2002) 121–134.
[22] T. Matsumoto, P. Suthiwarapirak, T. Kanda, Mechanisms of multiple cracking and fracture of DFRCC under fatigue flexure, J. Adv. Concr. Technol. 1 (3) (2003) 299–306.
[23] P. Suthiwarapirak, T. Matsumoto, Fiber bridging degradation based fatigue analysis of ECC under flexure, J. Appl. Mech. 6 (2003) 1179–1188.
[24] P. Suthiwarapirak, T. Matsumoto, T. Kanda, Multiple cracking and fiber bridging characteristics of engineered cementitious composites under fatigue flexure, J. Mater. Civil Eng. ASCE 16 (5) (2004) 433–443.
[25] W. Liu, S. Xu, Q. Li, Study on flexural fatigue life of ultra-high toughness cementitious composites under constant amplitude cyclic loading, J. Build. Struct. 33 (1) (2012) 119–127 in Chinese.
[26] J. Zhang, V.C. Li, Monotonic and fatigue performance in bending of fiber-reinforced engineered cementitious composite in overlay system, Cem. Concr. Res. 32 (3) (2002) 415–423.
[27] C.K.Y. Leung, Y.N. Cheung, J. Zhang, Fatigue enhancement of concrete beam with ECC layer, Cem. Concr. Res. 37 (5) (2007) 743–750.
[28] W. Liu, S. Xu, Q. Li, Flexural behaviour of UHTCC-layered concrete composite beam subjected to static and fatigue loads, Fatigue Fract. Eng. Mater. Struct. 36 (8) (2013) 738–749.
[29] P. Jun, V. Mechtcherine, Behaviour of strain-hardening cement-based composites (SHCC) under monotonic and cyclic tensile loading: part 1 - experimental investigations, Cem. Concr. Compos. 32 (10) (2010) 801–809.
[30] P. Jun, V. Mechtcherine, Behaviour of strain-hardening cement-based composites (SHCC) under monotonic and cyclic tensile loading: part 2: modeling, Cem. Concr. Compos. 32 (10) (2010) 810–818.
[31] B.H. Oh, Fatigue analysis of plain concrete in flexure, J. Struct. Eng. ASCE 112 (2) (1986) 273–288.
[32] B.H. Oh, Fatigue life distributions of concrete for various stress levels, ACI Mater. J. 88 (2) (1991) 122–128.
[33] H. Li, M. Zhang, J. Ou, Flexural fatigue performance of concrete containing nano-particles for pavement, Int. J. Fatigue 29 (7) (2007) 1292–1301.
[34] K. Aas-Jakobsen, Fatigue of concrete beams and columns, Bulletin No. 70-1, NTH Institute for Betonkonstruksjoner, Trondheim, September, 1970.

[35] B. Zhang, D.V. Phillips, K. Wu, Effects of loading frequency and stress reversal on fatigue life of plain concrete, Mag. Concr. Res. 48 (177) (1996) 361–375.
[36] M.T. Do, P.C. Chaallal Aïtcin, Fatigue behavior of high performance concrete, J. Mater. Civ. Eng. ASCE 5 (1993) 96–111.
[37] I.D. Karsan, J.O. Jirsa, Behavior of concrete under compressive loadings, J. Struct. Div. 95 (12) (1969) 2543–2564.
[38] C. Redon, V.C. Li, C. Wu, H. Hoshiro, T. Saito, A. Ogawa, Measuring and modifying interface properties of PVA fibers in ECC matrix, J. Mater. Civ. Eng. ASCE 13 (6) (2001) 399–406.
[39] Y. Song, Dynamic Constitutive Relation and Failure Criterion of Concrete 1, 2-3, Science Press, Beijing, 2012 114–116 in Chinese.